Effect of intramodal and intermodal nonlinearities on the flexural resonant frequencies of cantilevered beams

John E. Sader [1,*] Stefano Stassi [2] Carlo Ricciardi,[2] and Michael L. Roukes[3]

[1]*Graduate Aerospace Laboratories and Department of Applied Physics,*
California Institute of Technology, Pasadena, California 91125, USA
[2]*Department of Applied Science and Technology, Politecnico di Torino,*
Corso Duca Degli Abruzzi, 24, 10129 Torino, Italy
[3]*Departments of Physics, Applied Physics, and Bioengineering, California Institute of Technology,*
Pasadena, California 91125, USA

Sensing applications that utilize nanomechanical resonators require careful control of nonlinear effects in their eigenmodes to ensure robust measurement. While the effect of intra- and intermodal nonlinearities on the resonant frequencies of doubly clamped elastic beams have been widely studied using theory and experiment, commensurate studies on cantilevered beams are limited in comparison. Here, we present such a detailed study that includes an explicit and simple formula for the flexural resonant frequencies of slender cantilevered beams that accounts for intra- and intermodal nonlinearities. Using this general theory, numerical results for the modal nonlinear coefficients are tabulated for the first 20 flexural eigenmodes of cantilevered beams possessing uniform cross sections. The accuracy of this theory, and the effect of cantilever aspect ratio (length/width) on these nonlinear coefficients, is explored using high-accuracy laser Doppler vibrometry experiments. We anticipate that these results will find utility in single- and multimode applications, where the effect of finite oscillation amplitude on the cantilever resonant frequencies can significantly impact measurement design and interpretation.

I. INTRODUCTION

Recent advances in the development of micro- and nano-electromechanical systems (MEMS and NEMS, respectively) have enabled a multitude of high-resolution sensing applications, ranging from the detection of air-borne analytes to the imaging of surfaces with atomic resolution [1–7]. Miniaturization of mechanical resonators from macroscopic to nanometer length scales dramatically enhances the mass responsivity of the device due to an analyte adsorption event—varying as the reciprocal of the fourth power of the device size [8]. This has led to the development of highly sensitive nanomechanics-based mass spectrometry capable of detecting mass at the single nanoparticle and single molecule level [9–13]. Multimode detection has also enabled other analyte properties to be measured, including their stiffness and shape [14–18].

Fundamental to all these applications is a comprehensive understanding of the vibrational response of the resonator. Driving the device at small oscillation amplitude leads to operation in the quasilinear regime, facilitating interpretation of the measured resonant frequencies of a device. Even so, a nonlinear response is inevitable at any oscillation amplitude, which can modify the device sensitivity and the requisite theory for data analysis [19,20]. For example, multimodal detection of nanomechanical resonators has been used to measure the mass distribution of an analyte [16,21] and

characterize the nature of its interaction with the surrounding fluid [22]. These applications required the effect of inter- and intramodal nonlinearities to be negligible, which necessitated careful tuning of the experiments to ensure a linear response with no cross talk between the modes. Nonlinear effects thus pose a fundamental limit on device operation in practice, while simultaneously opening the door to the exploitation of unprecedentedly rich dynamical features including the possibility of enhanced measurement sensitivity [23]. Therefore, a comprehensive understanding of these nonlinear effects, and an ability to control them, is essential to enhancing measurement sensitivity, device performance, and generating new fields of application.

The Duffing resonator is a canonical model that incorporates a cubic nonlinearity into the usual simple harmonic oscillator. A hardening nonlinearity in the Duffing model accurately captures the resonance behavior of a slender doubly clamped elastic beam, where increasing the oscillation amplitude increases the resonant frequency of any single vibrational mode. This *intramodal* nonlinearity is driven by induced tension along the beam axis, which is controlled by the relative magnitude of the oscillation amplitude to the beam thickness and can be easily calculated using Euler-Bernoulli beam theory [24,25]. In contrast, a slender cantilevered elastic beam cannot sustain such axial tension yet also exhibits a weak hardening intramodal nonlinearity in its fundamental flexural mode, while higher-order flexural modes are strongly softening [26–28]. This nonlinearity in cantilevered beams is controlled by the beam length (not its thickness). Thus much higher amplitudes are needed to induce nonlinear

*jsader@caltech.edu

effects in cantilevered beams than those required for doubly clamped beams. The mechanisms driving intramodal nonlinearities in doubly clamped and cantilevered beams can also induce *intermodal* nonlinearities, where excitation of one vibrational mode affects the resonant frequencies of the other modes. Intermodal nonlinearities of the flexural modes of doubly clamped elastic beams have been studied both theoretically and experimentally, where excellent agreement has been reported [29–34]. In contrast, intramodal and particularly intermodal nonlinearities in cantilevered beams have received comparatively little attention [35–37]. One notable study on the effect of intermodal nonlinearities is that of Westra *et al.* [35] who primarily focused on the effect of flexural-torsional intermodal nonlinearities in cantilevered beams. While some comparison to experiment was reported, the study did not involve accurate calibration of the oscillation amplitude nor quantitative comparison between theory and measurement. Moreover, the theory was not reported in a form that facilitates implementation by practitioners.

We address this gap in the literature by reporting a comprehensive theory to describe the effect of intra- and intermodal nonlinearities on the flexural resonant frequencies of slender cantilevered beams of arbitrary cross section. This includes (1) a simple yet general analytical formula for beams of arbitrary cross section and (2) tabulated numerical nonlinear coefficients for beams of uniform cross section that facilitate implementation in practice. Specifically, in Sec. II we theoretically study the nonlinear response of slender cantilevered beams. In contrast to doubly clamped beams, the leading-order nonlinearity does not involve any induced tension but arises from enhancement and competition between inertia and stiffness of the beam at finite oscillation amplitude. This theory is then used to derive a simple analytical formula for the flexural resonant frequencies that accounts for intra- and intermodal nonlinearities. Numerical data for the modal nonlinear coefficients of a cantilevered beam of uniform cross section are reported for the first 20 modes. Then, in Sec. III, the developed theory and simple formula are experimentally validated using highly accurate measurements. This involves laser Doppler vibrometry (LDV) of microcantilever beams of uniform cross section and varying aspect ratio (length/width), facilitating rapid and accurate measurement of the oscillation amplitude. Details of the theoretical derivation reported in Sec. II are relegated to the Appendix.

II. THEORY

The theoretical framework in Ref. [38], for the nonlinear dynamics of a slender cantilevered beam whose cross section is uniform along its length, forms the basis for calculations reported in this study. This previous work is extended here to (1) a beam of arbitrary cross section and variation along the beam length in Sec. II A, which in turn is used to (2) formulate the required general theory for the effect of intra- and intermodal nonlinearities on the flexural resonant frequencies in Sec. II B. These two items form the principle theoretical contribution of this study, from which numerical results for modal nonlinear coefficients are reported and then compared to experiment.
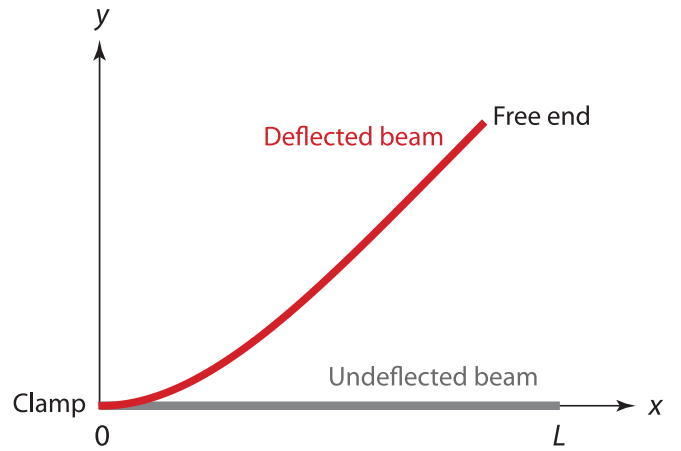

FIG. 1. Schematic showing the undeflected (gray) and deflected (red) slender cantilever beam of length, L, that is clamped at $x = 0$. The inextensible condition of the cantilever beam is illustrated by the fact that the total arc length of the beam is unchanged under deflection. The Cartesian coordinate system and its origin are indicated.

A. Action integral for nonlinear deflection

Consider a cantilevered beam of length, L, linear mass density, μ, Young's modulus, E, and areal moment of inertia, I. The action integral for the beam deflection function, y, follows from the theoretical framework of Ref. [38], which for a general beam with arbitrary cross-sectional variation along its length becomes

$$S(y) = \frac{L}{2} \int_{t_0}^{t_1} \int_0^1 \mu \left[\left(\frac{\partial y}{\partial t} \right)^2 + \frac{1}{4L^2} \left(\frac{\partial}{\partial t} \int_0^\zeta \left(\frac{\partial y}{\partial \zeta'} \right)^2 d\zeta' \right)^2 \right]$$
$$- \frac{EI}{L^4} \left(\frac{\partial^2 y}{\partial \zeta^2} \right)^2 \left(1 + \frac{1}{L^2} \left(\frac{\partial y}{\partial \zeta} \right)^2 \right) d\zeta \, dt, \tag{1}$$

where t is time, the limits of integration, t_0 and t_1, are arbitrary, $\zeta \equiv s/L$ is the dimensionless arc length along the cantilever beam from its clamped end, and s is the corresponding dimensional arc length. Only the leading-order nonlinear effect of finite deflection, y, is included in Eq. (1). It is assumed that the beam is inextensible, i.e., its axial strain is zero; see Fig. 1.

The first term in Eq. (1) (proportional to μ) is the kinetic energy density of the beam, whereas the second term is its strain energy density. Equation (1) thus shows that both the kinetic and strain energies are enhanced by finite deflection, with the length scale for onset of these nonlinear effects being the beam length, L; see the two terms with the prefactor $1/L^2$. Nonlinear enhancement of the kinetic energy is due to the motion of material points parallel to the undeflected beam axis, i.e., in the x direction; see Fig. 1. This effect is absent in the (linear) small-deflection limit where the beam moves in the (vertical) y direction only. In contrast, the increase in strain energy is due to beam curvature at finite deflection, i.e., a curved beam is stiffer than a straight beam. These enhancements in the kinetic and strain energies for finite (nonlinear) deformation arise from the inextensible property of a deflected cantilever beam.

B. Effect of intra- and intermodal nonlinearities on the resonant frequencies

Consider a deflection function, y, of the form

$$y(\zeta, t) = \Phi_m(\zeta)f_m(t) + \Phi_n(\zeta)f_n(t), \qquad (2)$$

where $\Phi_i(\zeta)$ are two eigenmodes $(i = m, n)$ of the cantilevered beam in the linear small-amplitude limit, with $i = 1, 2, 3, \ldots$, under the normalization $\Phi_i(\zeta_0) = 1$, ζ_0 is the measurement position, and $f_i(t)$ is the amplitude function of eigenmode i. Substituting Eq. (2) into Eq. (1) and using the orthogonal properties of the eigenmodes gives

$$S(y) = \frac{L}{2} \int_{t_0}^{t_1} \sum_{i=m,n} \left(I_i^{(1)} \dot{f}_i^2 + I_i^{(2)} f_i^2 \right)$$

$$+ \frac{1}{L^2} \sum_{i=m,n} \sum_{j=m,n} \sum_{p=m,n} \sum_{q=m,n}$$

$$\left(f_i \dot{f}_j f_p \dot{f}_q I_{ijpq}^{(3)} - f_i f_j f_p f_q I_{ijpq}^{(4)} \right) dt, \qquad (3)$$

where the time derivative $\dot{f}_i(t) \equiv df_i(t)/dt$ and

$$I_i^{(1)} = \int_0^1 \mu \Phi_i^2 \, d\zeta, \quad I_i^{(2)} = \int_0^1 \frac{EI}{L^4}(\Phi_i'')^2 \, d\zeta,$$

$$I_{ijpq}^{(3)} = \int_0^1 \mu \left(\int_0^\zeta \Phi_i' \Phi_j' \, d\xi \int_0^\zeta \Phi_p' \Phi_q' \, d\xi \right) d\zeta,$$

$$I_{ijpq}^{(4)} = \int_0^1 \frac{EI}{L^4} \Phi_i'' \Phi_j'' \Phi_p' \Phi_q' \, d\zeta, \qquad (4)$$

with the spatial derivative $\Phi_i'(\zeta) \equiv d\Phi_i(\zeta)/d\zeta$.

We choose the time dependencies of eigenmodes, m and n, to be

$$f_m(t) = A_m \cos(\omega_m t + \phi_m), \quad f_n(t) = A_n \cos(\omega_n t + \phi_n), \qquad (5)$$

where the resonant frequencies, ω_m and ω_n, are to be evaluated with $m \neq n$, the phases, ϕ_m and ϕ_n, are independent and arbitrary, and A_m and A_n are the amplitudes of eigenmodes m and n, respectively. Substituting Eq. (5) into Eq. (4) then gives the required leading-order result for the relative frequency shift of eigenmode, m, due to the intra- and intermodal nonlinearities,

$$\frac{\Delta \omega_m}{\omega_m^{(0)}} = X_m \left(\frac{A_m}{L} \right)^2 + (1 - \delta_{mn}) V_{mn} \left(\frac{A_n}{L} \right)^2, \qquad (6)$$

where $\Delta \omega_i \equiv \omega_i - \omega_i^{(0)}$, the linear resonant frequency of eigenmode, i, is $\omega_i^{(0)}$ $(i = m, n)$, δ_{mn} is the Kronecker delta function, and the modal nonlinear coefficients are

$$X_m = \frac{3I_{mmmm}^{(4)}}{I_m^{(2)}} - \frac{I_{mmmm}^{(3)}}{4I_m^{(1)}}, \qquad (7a)$$

$$V_{mn} = \frac{I_{mmnn}^{(4)} + 4I_{mnmn}^{(4)} + I_{nnmm}^{(4)}}{4I_m^{(2)}} - \left(1 + \frac{I_n^{(2)}}{I_n^{(1)}} \frac{I_m^{(1)}}{I_m^{(2)}} \right) \frac{I_{mnmn}^{(3)}}{4I_m^{(1)}}. \qquad (7b)$$

Note that the positive and negative terms in Eq. (7) arise from different physical mechanisms. The (first) positive terms are due to the nonlinear enhancement of beam stiffness and define a hardening nonlinearity, whereas the (second) negative terms arise from the increase in beam inertia and are softening.

These terms compete to define the overall nonlinear response that can be either hardening or softening; as we show below, intermodal nonlinearities always produce a softening effect, i.e., $V_{mn} < 0$.

The intermodal contribution in Eq. (6) is independent of A_m, i.e., the amplitude of eigenmode m. Equation (6) can therefore be generalized to an arbitrary number of eigenmodes by superposition, giving

$$\frac{\Delta \omega_m}{\omega_m^{(0)}} = X_m \left(\frac{A_m}{L} \right)^2 + \sum_{\substack{n=1 \\ (n \neq m)}}^{\infty} V_{mn} \left(\frac{A_n}{L} \right)^2, \qquad (8)$$

where $m \geqslant 1$.

C. Cantilevered beam of uniform cross section

We apply the developed theory to a beam of uniform cross section and a measurement position of $\zeta_0 = 1$, i.e., the free end of the cantilevered beam. The required eigenmodes are

$$\Phi_i(\zeta) = \frac{(-1)^i}{2} \Bigg(\cos(C_i \zeta) - \cosh(C_i \zeta)$$

$$+ \frac{\cos C_i + \cosh C_i}{\sin C_i + \sinh C_i} [\cos(C_i \zeta) - \cosh(C_i \zeta)] \Bigg), \quad (9)$$

with eigenvalues given by

$$\cosh C_i \cos C_i = -1, \qquad (10)$$

for $i = 1, 2, 3, \ldots$. The required coefficients for the intra- and intermodal nonlinearities, X_m and V_{mn}, respectively, are then obtained by substituting Eq. (9) into Eq. (7).

The intramodal nonlinear coefficient, X_m, grows rapidly with m and has the high-mode-number asymptotic form,

$$X_m \sim -\frac{\pi^4 m^4}{48}, \quad m \gg 1, \qquad (11)$$

which is derived using the corresponding asymptotic expression for the eigenmodes,

$$\Phi_m(\zeta) \sim \frac{(-1)^{m+1}}{\sqrt{2}} \sin\left(\pi \left[\left(m - \frac{1}{2} \right) \zeta - \frac{1}{4} \right] \right), \quad m \gg 1. \qquad (12)$$

The boundary layers near the clamped and free ends, $\zeta = 0$ and 1, respectively, are ignored. Equation (11) establishes that the effect of the intramodal nonlinearities on the flexural resonant frequencies increases strongly with mode number, m.

Combining Eq. (11) with accurate numerical solutions for X_m, using the true eigenmodes in Eq. (9), allows a semiempirical expression to be formulated,

$$X_m \approx -0.574456 + 3.85554\,m - 7.22798\,m^2 + 5.99564\,m^3$$

$$- 2.02936\,m^4, \qquad (13)$$

that exhibits a maximum error of $<3\%$ for all m; see Fig. 2. This simple formula facilitates application in practice.
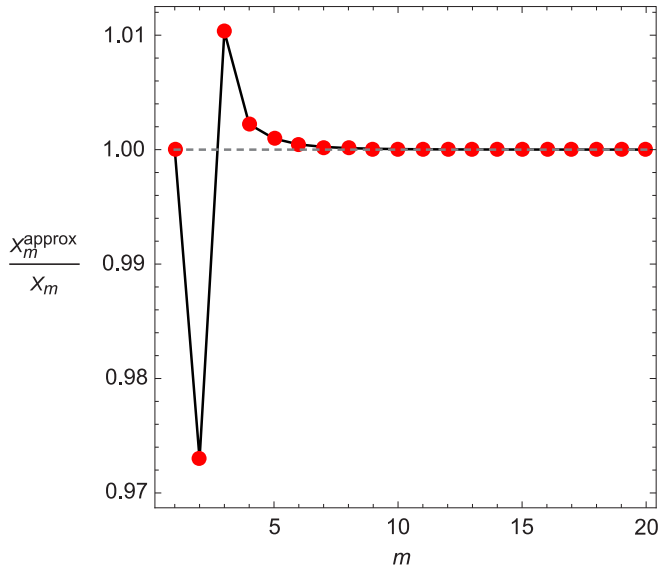
FIG. 2. Relative error of the approximate formula for the intramodal nonlinear coefficient, Eq. (13), as a function of mode number, m.

Similarly, we find the following asymptotic solution for the intermodal nonlinear coefficient:

$$V_{mn} \sim -\frac{\pi^2}{16}\left(\frac{n}{m}\right)^2$$
$$\times \frac{m^6 - 2m^5n + 3m^4n^2 + 3m^2n^4 - 2mn^5 + n^6}{(m^2 - n^2)^2},$$
$$m, n \gg 1, \quad (14)$$

which is strictly negative. The quadratic term, $(n/m)^2$, on the right-hand side of Eq. (14) is not symmetric in m and n, while the remaining term is symmetric. This shows that in the large-mode-number limit, the magnitude of V_{mn} generally increases with mode number of the excited eigenmode, n, and decreases with the mode number of the detected eigenmode, m. Moreover, the intermodal nonlinear coefficient is enhanced by choosing $m \approx n$. These general observations can be utilized in practice to control the effect of intermodal nonlinearities. In contrast to the asymptotic solution for the intermodal coefficient in Eq. (11), the complexity of Eq. (14) hinders the development of a simple approximate expression that is accurate for all m, n.

Numerical results for the intermodal nonlinear coefficients, X_m, and the corresponding intermodal coefficients, V_{mn}, are given in Tables I and II, respectively, for the first 20 flexural modes. The reported data sets are normalized by the corresponding asymptotic expressions for large mode number. These results confirm the validity of the large-mode-number asymptotic solutions in Eqs. (11) and (14) and show that nonlinear effects in slender cantilevered beams of uniform cross section are predominantly softening. The single exception is for the intramodal nonlinearity of the fundamental mode, $m = 1$. For this special case, contributions from nonlinear inertia and nonlinear stiffness are finely balanced, with stiffness dominating and producing a weak hardening response. Generally, the effects of nonlinear inertia are enhanced with

TABLE I. Scaled intramodal nonlinear coefficient, $\bar{X}_m \equiv X_m/X_m^{\mathrm{asym}}$, for a cantilevered beam of uniform cross section, where X_m^{asym} is the large-m asymptotic solution in Eq. (11).

m	$\bar{X}_m$	m	$\bar{X}_m$
1	−0.00955158	11	0.759420
2	0.198783	12	0.777430
3	0.340546	13	0.792946
4	0.454406	14	0.806448
5	0.536316	15	0.818304
6	0.597681	16	0.828797
7	0.645052	17	0.838147
8	0.682615	18	0.846531
9	0.713083	19	0.854092
10	0.738267	20	0.860944

mode number, m, leading to strong intramodal softening for $m \geqslant 2$. The situation is more complicated for the intermodal nonlinearities, as is evident from Eq. (14), the data set in Table II, and the discussion above.

III. EXPERIMENTAL VERIFICATION

Next, we report an experimental protocol to accurately measure the nonlinear response of a nanomechanical device and thereby assess the validity of the reported theoretical model.

This assessment is performed on cantilevers of varying slenderness, i.e., aspect ratio, AR = length/width. A commercial atomic force microscope (AFM) chip is used, which contains three tipless single-crystal-silicon cantilevers that have been precisely micromachined to a rectangular parallelepiped geometry; see Fig. 3. All these cantilevers have identically constant widths of 29 μm and thicknesses of 2 μm and thus present a uniform cross section as per the theoretical results and data set reported in Sec. II C. These cantilevers are denoted by their lengths of 396 μm (long), 193 μm (medium), and 94 μm (short). Therefore, their aspect ratios are AR = 14 (long), 6.6 (medium), and 3.2 (short). The cantilever
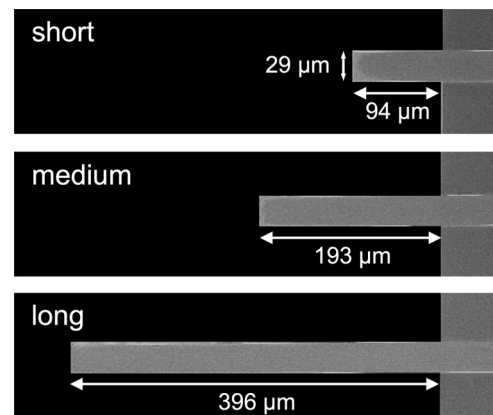
FIG. 3. Scanning electron micrographs of the three microcantilevers used in Sec. III, with the measured length and width of each cantilever indicated; all microcantilevers are of width, 29 μm, and have a nominal thickness of 2 μm.

TABLE II. Scaled intermodal nonlinear coefficient, $V_{mn}/V_{mn}^{\text{asymp}}$, for a cantilevered beam of uniform cross section, where V_{mn}^{asymp} is the large mode number asymptotic solution in Eq. (14).

										n										
m	1	2	3	4	5	6	7	8	9	10	11	12	13	14	15	16	17	18	19	20
1	NA	0.181536	0.913752	0.697795	0.548215	0.408172	0.318249	0.250220	0.202805	0.166445	0.139415	0.118038	0.101387	0.0878430	0.0769216	0.0678303	0.0603029	0.0539166	0.0485180	0.0438655
2	0.0739568	NA	0.0851124	0.954959	0.917832	1.04209	0.879624	0.795278	0.665388	0.580479	0.493607	0.431392	0.373582	0.329717	0.290140	0.258855	0.230851	0.208028	0.187595	0.170543
3	0.240372	0.0549583	NA	0.195532	0.923310	0.860550	1.20995	1.08995	1.12706	0.988439	0.931499	0.816328	0.747909	0.660776	0.601485	0.536751	0.489239	0.440812	0.403451	0.366676
4	0.151079	0.507510	0.160930	NA	0.304233	0.891432	0.789944	1.20407	1.11396	1.27013	1.15315	1.16505	1.04869	1.00713	0.907108	0.853024	0.771956	0.720181	0.655718	0.610550
5	0.106043	0.435792	0.678929	0.271808	NA	0.391209	0.878217	0.753285	1.15936	1.07697	1.30393	1.20885	1.29058	1.18627	1.18844	1.08877	1.05642	0.968676	0.925051	0.850850
6	0.0733668	0.459774	0.588000	0.740065	0.363524	NA	0.460396	0.874485	0.738841	1.11440	1.03034	1.28789	1.20665	1.34093	1.25106	1.29839	1.20630	1.20414	1.11720	1.09089
7	0.0543260	0.368572	0.785148	0.622819	0.775016	0.437236	NA	0.516116	0.875440	0.736508	1.07785	0.990070	1.25429	1.17993	1.34728	1.26922	1.35454	1.27220	1.30142	1.21964
8	0.0411091	0.320716	0.680719	0.913676	0.639800	0.799306	0.496734	NA	0.561730	0.878644	0.740449	1.04986	0.958972	1.21756	1.14593	1.33098	1.26106	1.37453	1.30128	1.35857
9	0.0323501	0.260529	0.683419	0.820713	0.956057	0.655678	0.818054	0.545390	NA	0.599662	0.882865	0.747520	1.02879	0.936026	1.18336	1.11244	1.30465	1.23983	1.37222	1.30628
10	0.0259346	0.222013	0.585467	0.914073	0.867521	0.966033	0.672271	0.833304	0.585757	NA	0.631654	0.887469	0.756036	1.01294	0.919478	1.15345	1.08245	1.27518	1.21333	1.35722
11	0.0213121	0.185217	0.541306	0.814192	1.03047	0.876276	0.965235	0.688959	0.846084	0.619708	NA	0.658975	0.892128	0.765082	1.00098	0.907734	1.12799	1.05675	1.24604	1.18584
12	0.0177607	0.159328	0.466923	0.809667	0.940319	1.07810	0.872691	0.961506	0.705119	0.857001	0.648618	NA	0.682565	0.896673	0.774164	0.991906	0.899540	1.10656	1.03520	1.21884
13	0.0150527	0.136146	0.422113	0.719128	0.990578	0.996694	1.09092	0.866611	0.957559	0.720394	0.866457	0.673509	NA	0.703129	0.901019	0.783019	0.984984	0.893961	1.08860	1.01734
14	0.0128940	0.118797	0.368704	0.682793	0.900184	1.09504	1.01460	1.08781	0.861332	0.954238	0.734635	0.874737	0.695151	NA	0.721211	0.905130	0.791508	0.979683	0.890310	1.07353
15	0.0111800	0.103511	0.332326	0.608946	0.892978	1.01162	1.14713	1.01376	1.07824	0.857687	0.951713	0.747812	0.882051	0.714132	NA	0.737230	0.908994	0.799571	0.975617	0.888085
16	0.00977415	0.0915580	0.294017	0.567729	0.811071	1.04089	1.07140	1.16737	1.00493	1.06671	0.855654	0.949927	0.759962	0.888560	0.730909	NA	0.751518	0.912614	0.807185	0.972497
17	0.00862383	0.0810361	0.265967	0.509893	0.781027	0.959755	1.13478	1.09769	1.16966	0.993487	1.05524	0.854962	0.948758	0.771149	0.894392	0.745841	NA	0.764340	0.916001	0.814353
18	0.00765883	0.0725347	0.238033	0.472505	0.711355	0.951610	1.05866	1.18844	1.10409	1.16253	0.981967	1.04467	0.855309	0.948083	0.781451	0.899647	0.759214	NA	0.775909	0.919167
19	0.00685066	0.0650183	0.216553	0.427633	0.675248	0.877614	1.07648	1.11837	1.21467	1.09951	1.15092	0.971449	1.03529	0.856430	0.947794	0.790947	0.904406	0.771259	NA	0.786399
20	0.00616037	0.0587898	0.195754	0.396032	0.617739	0.852333	1.00340	1.16131	1.15007	1.22328	1.08941	1.13762	0.962307	1.02711	0.858110	0.947800	0.799713	0.908736	0.782163	NA

TABLE III. Comparison of the measured intramodal nonlinear coefficients, X_m^{expt}, of the three cantilevers, to the (infinite aspect ratio) theoretical model of Sec. II C, X_m^{theory}. Results are given to three significant figures for the first three flexural modes, except for the smallest AR due to overlap of the flexural and torsional resonances. Listed uncertainties represent a 95% confidence interval arising from least-squares fits to the measured amplitude responses; see Fig. 4.

Mode, m	X_m^{theory}	X_m^{expt}		
		AR = 3.2 (short)	AR = 6.6 (medium)	AR = 14 (long)
1	0.0194	0.0143 ± 0.0017	0.0170 ± 0.0031	0.0170 ± 0.0031
2	-6.45	-12.1 ± 2.2	-7.03 ± 1.01	-6.27 ± 0.19
3	-56.0		-64.9 ± 3.1	-56.9 ± 1.41

dimensions are measured using a Zeiss MERLIN field emission scanning electron microscope, the results of which are reported in Fig. 3.

The AFM cantilever chip is mounted with carbon adhesive tape on a piezoelectric disk that is used for actuation. This system is contained in a vacuum chamber. All the measurements are performed at room temperature and an air pressure of 2×10^{-7} mbar, which is achieved using a vacuum system comprising a membrane and turbomolecular pump (HiCube80 Eco, Pfeiffer). The vibrational amplitude response of the cantilevers is measured with a laser Doppler vibrometer (LDV, MSA-500, Polytec Gmbh) coupled with a lock-in amplifier (HF2LI, Zurich Instruments). The lock-in amplifier is used both for piezodisk actuation and for LDV signal analysis, with the procedure described below. Specifically, the lock-in amplifier sweeps the frequency around the investigated resonance mode and records the output of the LDV, which is intrinsically amplitude calibrated and linear within the amplitude range investigated. The drive frequency is initially swept upwards and downwards to identify whether the nonlinearity of the mode in question is hardening or softening in nature. The frequency sweep direction is then chosen to be upwards/downwards for an initially observed hardening/softening nonlinearity. This enables unambiguous measurement of the resonant frequency, which coincides with the frequency of maximal oscillation amplitude.

A. Intramodal nonlinearity

Simultaneously measuring the resonant frequency, ω_m, of each eigenmode of the cantilever and the oscillation amplitude at this resonance, A_m, allows the intramodal nonlinear coefficient, X_m^{expt}, to be experimentally determined using

$$\frac{\Delta\omega_m}{\omega_m^{(0)}} = X_m^{\text{expt}} \left(\frac{A_m}{L}\right)^2, \qquad (15)$$

where $\Delta\omega_m \equiv \omega_m - \omega_m^{(0)}$. A sample measurement for the first flexural mode, $m = 1$, of the short cantilever is given in Fig. 4. Using the same approach, intramodal nonlinear coefficients are measured for the first three flexural eigenmodes of the medium and long cantilevers. The third flexural eigenmode of the short cantilever cannot be measured robustly because this flexural mode and the first torsional mode have similar resonant frequencies.

The measured intramodal nonlinear coefficients, X_m^{expt}, are reported in Table III along with a comparison to the (infinite aspect ratio) theory of Sec. II C. Good agreement is evident

between theory and measurement, especially at the largest aspect ratio of AR = 14. Reducing the cantilever aspect ratio and/or increasing its mode number (which reduces its effective aspect ratio) makes the intramodal nonlinear coefficients more negative, i.e., more softening. This is true for all measured eigenmodes, $m = 1, 2, 3$.

Interestingly, the degree of softening in measurements of the fundamental flexural mode (for cantilevers of uniform cross section) with decreasing aspect ratio is less than that reported in Ref. [27] (for cantilevers of nonuniform cross section). In the present measurements, this intramodal nonlinearity is always a hardening phenomenon, i.e, $X_1^{\text{expt}} > 0$, whereas in Ref. [27] it becomes softening, i.e., $X_1^{\text{expt}} < 0$, for AR $\lesssim 8$. Combining these independent measurements on different cantilever types (uniform and nonuniform cross sections) leads to the conclusion that the hardening/softening nature of the fundamental flexural mode can be controlled by
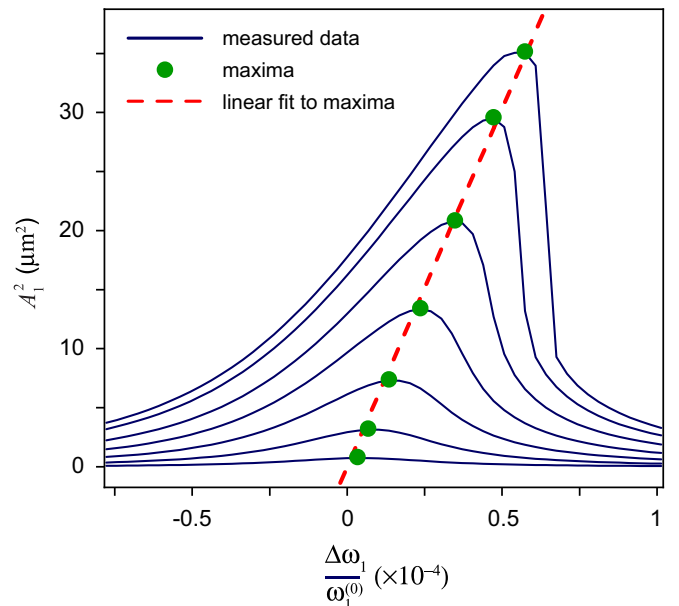
FIG. 4. Measured intramodal nonlinear coefficient, X_1^{expt}, of the short cantilever, i.e., for eigenmode, $m = 1$. Solid (blue) curves are measured data of the squared amplitude response of the free end of the cantilever, as the drive amplitude is increased (bottom to top). The solid (green) dots denote the maxima of the amplitude responses (where the resonant frequencies are measured) and the straight (red) dashed line is a linear fit to these maxima; the latter is used to determine X_1^{expt} from Eq. (15).
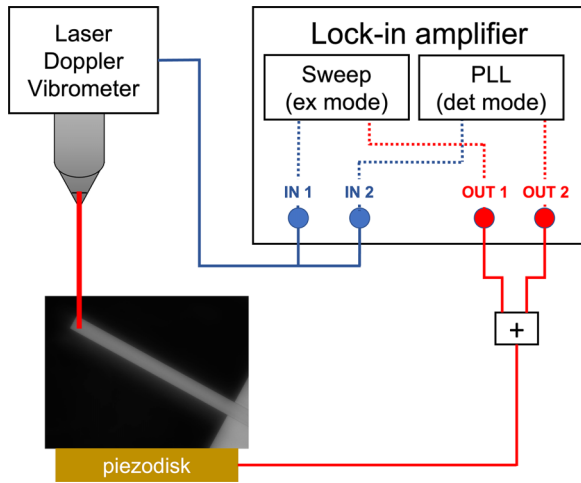
FIG. 5. Experimental setup to measure the intermodal nonlinear coefficients. Oscillation amplitude of a cantilever is measured using LDV and acquired by a lock-in amplifier. The lock-in amplifier is used to sweep the drive frequency of the excited eigenmode, n, and measure the resonant frequency of a different detected eigenmode, m, with a digital PLL. Mechanical excitation of the cantilever is performed using a piezoelectric shaker which is controlled by lock-in outputs.

varying the cantilever cross section along its length. This is not unexpected given the fine balance between the effects of nonlinear stiffness (hardening) and nonlinear inertia (softening) in the fundamental flexural mode; see discussion in Sec. II C.

B. Intermodal nonlinearity

To measure the intermodal nonlinear coefficients, we employ two input and two output channels of the lock-in amplifier; see Fig. 5. This configuration is used to detect the frequency shift of one eigenmode that is induced by the excitation of another eigenmode. Specifically, one set of input/output channels is engaged to excite and sweep the frequency of eigenmode, n, for which its oscillation amplitude is measured using the LDV. The second set of input/output channels runs a digital phase locked loop (PLL) that excites and detects the resonant frequency of another eigenmode, m. Note that the excited and detected eigenmodes differ, i.e., $m \neq n$.

The detected eigenmode, m, is driven at low amplitude so that it remains in its quasilinear regime, i.e., its resonant frequency is independent of its oscillation amplitude. This avoids any significant effect from its intramodal nonlinearity. In contrast, the excited eigenmode, n, is driven at relatively large amplitude to generate a large frequency shift and facilitate measurement. The required intermodal nonlinear coefficient, V_{mn}^{expt}, is then determined using

$$\frac{\Delta \omega_m}{\omega_m^{(0)}} = V_{mn}^{\mathrm{expt}} \left(\frac{A_n}{L} \right)^2, \quad m \neq n, \qquad (16)$$

by overlaying (1) the fractional frequency shift of eigenmode, m, with (2) the oscillation amplitude squared of eigenmode, m, both as functions of the drive frequency of eigenmode,

TABLE IV. Comparison of the measured intermodal nonlinear coefficients, V_{mn}^{expt}, to the (infinite aspect ratio) theoretical model of Sec. II C (values in parentheses). Results are reported to three significant figures. The indices, m and n, correspond to the detected and excited eigenmodes, respectively. Listed uncertainties represent a 95% confidence interval arising from the least-squares fits.

	m	n 1	2	3
AR = 14	1	NA	-2.77 ± 0.04 (-2.84)	-41.6 ± 0.6 (-40.3)
	2	-0.0702 ± 0.0009 (-0.0722)	NA	-5.07 ± 0.24 (-4.88)
	3	-0.124 ± 0.002 (-0.131)	-0.660 ± 0.007 (-0.623)	NA
AR = 6.6	1	NA	-3.10 ± 0.06 (-2.84)	-53.8 ± 0.6 (-40.3)
	2	-0.0718 ± 0.0048 (-0.0722)	NA	-6.63 ± 0.17 (-4.88)
	3	-0.113 ± 0.013 (-0.131)	-0.691 ± 0.004 (-0.623)	NA
AR = 3.2	1	NA	-4.00 ± 0.24 (-2.84)	
	2	-0.0751 ± 0.0022 (-0.0722)	NA	
	3			NA

n. The single adjustable parameter, V_{mn}^{expt}, in Eq. (16) is used to achieve this overlay using a least-squares fit. A sample measurement from this protocol is given in Fig. 6, showing a precise overlap in accordance with Eq. (16). To ensure a linear response in eigenmode, m, this measurement protocol is repeated for four small but different drive amplitudes of eigenmode, m.

Intermodal coefficients, V_{mn}^{expt}, are measured for all permutations, (m, n), of the first three flexural eigenmodes of the long and medium cantilevers. For the short cantilever, V_{12}^{expt} and V_{21}^{expt} only are measured—this is for the same reason the intramodal nonlinear coefficient of eigenmode 3 is not measured; see Sec. III A. Table IV gives the measurement data set and provides a comparison with the (infinite aspect ratio) theoretical predictions in Table II. Good agreement is observed throughout, with discrepancy increasing as the aspect ratio is reduced or the eigenmode numbers increased. This is similar to observations for the intramodal nonlinearity reported in Sec. III A and is consistent with the overriding large-aspect-ratio assumption of the theoretical model.

IV. CONCLUSIONS

Nonlinearities in the eigenmodes of resonant mechanical sensors intrinsically control the dynamic range over which quasilinear measurements can be performed. Knowledge of this phenomenon is therefore critical in experimental design and operation. We have reported a detailed theoretical and experimental investigation of the modal nonlinearities in cantilevered beams. Analytical formulas for the effect of intra- and intermodal nonlinearities, on the flexural resonant
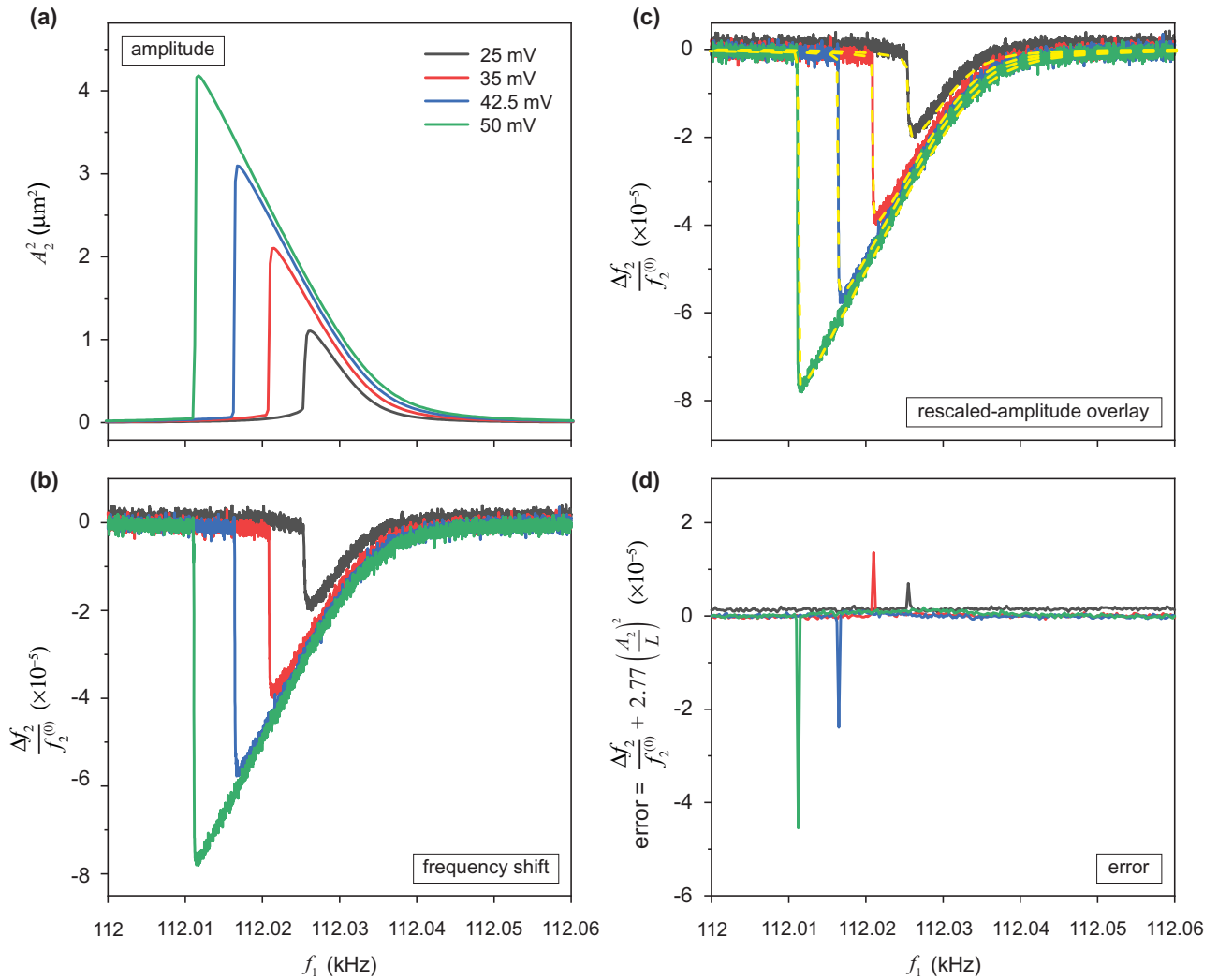
FIG. 6. Measurement of the intermodal nonlinear coefficient, V_{21}^{expt}, for the long cantilever, i.e., the detected eigenmode is $m = 2$ and the excited eigenmode is $n = 1$; $\omega_i = 2\pi f_i$. (a) Squared oscillation amplitude curves of the detected eigenmode, $m = 2$, and (b) its fractional frequency shift, measured by sweeping the drive frequency around the resonant frequency of the excited eigenmode, $n = 1$. Measurements taken for different drive voltages applied to the piezoshaker, as indicated in (a). (c) The squared oscillation amplitude curves in (a) are rescaled (dashed yellow curves) to overlap with the frequency shift curves in (b). This gives the intermodal nonlinear coefficient $V_{21}^{\text{expt}} = -2.77 \pm 0.04$ via Eq. (16). (d) Residual error of the fractional frequency shift and rescaled amplitude curves in (c); spikes correspond to slight mismatches between the vertical jumps in (c).

frequencies of a slender cantilever beam of arbitrary cross section, were derived. This theory was applied to a cantilever of uniform cross section, for which (1) simple asymptotic formulas in the high-mode-number limit and (2) accurate tabulated numerical data for the first 20 eigenmodes were presented. Both intra- and intermodal nonlinearities were found to induce a softening effect, with the singular exception of the intramodal nonlinearity of the fundamental flexural mode which is weakly hardening.

An experimental protocol was developed to accurately measure the oscillation amplitudes and resonant frequencies of cantilevered beams. This allowed for a rigorous assessment of the developed theory. Specifically, this protocol was applied to three cantilevers of varying aspect ratio, for which good agreement with theory was observed, especially for cantilevers of large aspect ratio. Decreasing the aspect ratio was found to enhance the softening nonlinearity in all cases. A

theory for this aspect ratio phenomenon is yet to be reported and represents an area of future work.

This study shows that elastic beam theory can be used with confidence to calculate the effect of modal nonlinearities in slender cantilevered beams with finite aspect ratio, which has immediate implications to the development of highly sensitive nanoelectromechanical sensors.

APPENDIX: DERIVATION OF THE MODAL NONLINEARITY THEORY

In this Appendix, we present derivation details of (1) the leading-order nonlinear response of a slender cantilevered beam and (2) formulas for the effect of modal nonlinearities on the flexural resonant frequencies, reported in Sec. II. This utilizes the theoretical framework of Ref. [38]. It is assumed that the beam is inextensible, i.e., its axial strain is zero.

1. Action integral

The kinetic energy of the beam is

$$T = \frac{L}{2} \int_0^1 \mu \left| \frac{\partial \mathbf{u}(\zeta, t)}{\partial t} \right|^2 d\zeta, \tag{A1}$$

where

$$\mathbf{u}(\zeta, t) = X(\zeta, t)\mathbf{i} + Y(\zeta, t)\mathbf{j}, \tag{A2}$$

is the local displacement vector of any material point along the beam with respect to its initial (undeformed) position, $\mathbf{i}$ and $\mathbf{j}$ are the Cartesian basis vectors in the x and y directions, respectively, and X and Y are the corresponding Lagrangian displacement variables; see Fig. 1. The strain energy is

$$V = \frac{L}{2} \int_0^1 EI \kappa^2(\zeta, t) d\zeta, \tag{A3}$$

where κ is the local curvature of the beam's neutral axis. All symbols are as defined in Sec. II.

The shape of the deformed beam is parametrized by the dimensionless arc length, ζ, to give

$$\mathbf{r} = x(\zeta, t)\mathbf{i} + y(\zeta, t)\mathbf{j}, \tag{A4}$$

where (x, y) are the Cartesian coordinates of the (fixed) inertial frame, as per Fig. 1. This is directly related to the Lagrangian displacement variables in Eq. (A2) via

$$x(\zeta, t) = \zeta L + X(\zeta, t), \quad y(\zeta, t) = Y(\zeta, t). \tag{A5}$$

The general expression for the curvature is

$$\kappa = \frac{\dfrac{\partial x}{\partial \zeta} \dfrac{\partial^2 y}{\partial \zeta^2} - \dfrac{\partial y}{\partial \zeta} \dfrac{\partial^2 x}{\partial \zeta^2}}{\left[\left(\dfrac{\partial x}{\partial \zeta} \right)^2 + \left(\dfrac{\partial y}{\partial \zeta} \right)^2 \right]^{\frac{3}{2}}}. \tag{A6}$$

However, because ζ is the dimensionless arc length, it follows that

$$\left(\frac{\partial x}{\partial \zeta} \right)^2 + \left(\frac{\partial y}{\partial \zeta} \right)^2 = L^2 \tag{A7}$$

and Eq. (A6) simplifies,

$$\kappa = \frac{1}{L^3} \left(\frac{\partial x}{\partial \zeta} \frac{\partial^2 y}{\partial \zeta^2} - \frac{\partial y}{\partial \zeta} \frac{\partial^2 x}{\partial \zeta^2} \right). \tag{A8}$$

Rearranging Eq. (A7) produces the following leading-order asymptotic expressions in the limit of small deflection:

$$\frac{\partial x}{\partial \zeta} = L \left(1 - \frac{1}{2L^2} \left(\frac{\partial y}{\partial \zeta} \right)^2 + \cdots \right), \quad \frac{\partial^2 x}{\partial \zeta^2} = -\frac{1}{L} \frac{\partial^2 y}{\partial \zeta^2} \frac{\partial y}{\partial \zeta} + \cdots. \tag{A9}$$

Substituting Eq. (A9) into Eq. (A8) gives the required leading-order expression for the curvature,

$$\kappa = \frac{1}{L^2} \frac{\partial^2 y}{\partial \zeta^2} \left(1 + \frac{1}{2L^2} \left(\frac{\partial y}{\partial \zeta} \right)^2 + \cdots \right). \tag{A10}$$

Similarly, substituting Eq. (A5) into Eq. (A7) gives

$$\left(L + \frac{\partial X}{\partial \zeta} \right)^2 + \left(\frac{\partial y}{\partial \zeta} \right)^2 = L^2, \tag{A11}$$

which upon solution for X (again in the asymptotic limit of small $\partial y/\partial \zeta$) while imposing the clamp condition, $X(0, t) = 0$, produces the leading-order asymptotic result,

$$X(\zeta, t) = -\frac{1}{2L} \int_0^\zeta \left(\frac{\partial y}{\partial \zeta'}\right)^2 d\zeta' + \cdots. \tag{A12}$$

The required leading-order expressions for the kinetic energy and strain energy of the beam are then obtained by substituting Eqs. (A5) and (A12) into Eq. (A1), and Eq. (A10) into Eq. (A3), respectively,

$$T = \frac{L}{2} \int_0^1 \mu \left[\left(\frac{\partial y}{\partial t}\right)^2 + \frac{1}{4L^2}\left(\frac{\partial}{\partial t}\int_0^\zeta \left(\frac{\partial y}{\partial \zeta'}\right)^2 d\zeta'\right)^2\right] d\zeta, \tag{A13a}$$

$$V = \frac{1}{2L^3} \int_0^1 EI \left(\frac{\partial^2 y}{\partial \zeta^2}\right)^2 \left(1 + \frac{1}{L^2}\left(\frac{\partial y}{\partial \zeta}\right)^2\right) d\zeta. \tag{A13b}$$

The action, $S(y) \equiv \int_{t_0}^{t_1} T - V \, dt$, where the limits of integration, t_0 and t_1, are arbitrary, then follows from Eqs. (A13),

$$S(y) = \frac{L}{2} \int_{t_0}^{t_1} \int_0^1 \mu \left[\left(\frac{\partial y}{\partial t}\right)^2 + \frac{1}{4L^2}\left(\frac{\partial}{\partial t}\int_0^\zeta \left(\frac{\partial y}{\partial \zeta'}\right)^2 d\zeta'\right)^2\right] - \frac{EI}{L^4}\left(\frac{\partial^2 y}{\partial \zeta^2}\right)^2 \left(1 + \frac{1}{L^2}\left(\frac{\partial y}{\partial \zeta}\right)^2\right) d\zeta \, dt. \tag{A14}$$

2. Effect of modal nonlinearities on the flexural resonant frequencies

We consider a deflection function,

$$y(\zeta, t) = \Phi_m(\zeta) f_m(t) + \Phi_n(\zeta) f_n(t), \tag{A15}$$

where all symbols in this section are as defined in Sec. II. Substituting Eq. (A15) into Eq. (A14) gives

$$S(y) = \frac{L}{2} \int_{t_0}^{t_1} \sum_{i=m,n} \left(I_i^{(1)} \dot{f}_i^2 + I_i^{(2)} f_i^2\right) + \frac{1}{L^2} \sum_{i=m,n} \sum_{j=m,n} \sum_{p=m,n} \sum_{q=m,n} \left(f_i \dot{f}_j f_p \dot{f}_q I_{ijpq}^{(3)} - f_i f_j f_p f_q I_{ijpq}^{(4)}\right) dt, \tag{A16}$$

where

$$I_i^{(1)} = \int_0^1 \mu \Phi_i^2 \, d\zeta, \quad I_i^{(2)} = \int_0^1 \frac{EI}{L^4}\left(\Phi_i''\right)^2 d\zeta,$$

$$I_{ijpq}^{(3)} = \int_0^1 \mu \left(\int_0^\zeta \Phi_i' \Phi_j' \, d\xi \int_0^\zeta \Phi_p' \Phi_q' \, d\xi'\right) d\zeta,$$

$$I_{ijpq}^{(4)} = \int_0^1 \frac{EI}{L^4} \Phi_i'' \Phi_j'' \Phi_p' \Phi_q' \, d\zeta. \tag{A17}$$

The integrals in Eq. (A17) possess strong symmetries with respect to their indices. This property is used in the derivation of Eq. (A16). The governing equations for $f_m(t)$ and $f_n(t)$ are calculated by finding the extremum of Eq. (A16) via the Euler-Lagrange equations, yielding

$$I_m^{(1)} f_m''(t) + I_m^{(2)} f_m(t) + \frac{1}{L^2} g_{mn}(t) = 0, \tag{A18}$$

with

$$\begin{aligned}
g_{mn}(t) = {}&\left(I_{mmmm}^{(3)} f_m''(t) + I_{mmmn}^{(3)} f_n''(t)\right) f_m^2(t) \\
&+ \left[2I_{mmmn}^{(3)} f_m''(t) + \left(I_{mmnn}^{(3)} + I_{mnmn}^{(3)}\right) f_n''(t)\right] f_m(t) f_n(t) \\
&+ \left(I_{mnmn}^{(3)} f_m''(t) + I_{nnmn}^{(3)} f_n''(t)\right) f_n^2(t) \\
&+ \left(I_{mmmm}^{(3)} \left[f_m'(t)\right]^2 + 2I_{mmmn}^{(3)} f_m'(t) f_n'(t) + I_{mmnn}^{(3)} \left[f_n'(t)\right]^2\right) f_m(t) \\
&+ \left(I_{mmmn}^{(3)} \left[f_m'(t)\right]^2 + 2I_{mnmn}^{(3)} f_m'(t) f_n'(t) + I_{nnmn}^{(3)} \left[f_n'(t)\right]^2\right) f_n(t) \\
&+ 2I_{mmmm}^{(4)} f_m^3(t) + 3\left(I_{mmmn}^{(4)} + I_{mnmm}^{(4)}\right) f_m^2(t) f_n(t) \\
&+ \left(I_{mmnn}^{(4)} + 4I_{mnmn}^{(4)} + I_{nnmm}^{(4)}\right) f_m(t) f_n^2(t) + \left(I_{mnnn}^{(4)} + I_{nnmn}^{(4)}\right) f_n^3(t), \tag{A19}
\end{aligned}$$

where the governing equation for f_n is obtained by swapping the m and n indices in Eqs. (A18) and (A19).

Next, we substitute

$$f_m(t) = A_m \cos(\omega_m t + \phi_m), \quad f_n(t) = A_n \cos(\omega_n t + \phi_n), \tag{A20}$$

into the governing differential equations for $f_m(t)$ and $f_n(t)$, and collecting harmonic terms at frequencies, ω_m and ω_n, respectively, to give

$$\omega_m^2 \frac{I_m^{(1)}}{I_m^{(2)}} - 1 = \left(\frac{A_m}{L}\right)^2 \left(\frac{3I_{mmmm}^{(4)} - \omega_m^2 I_{mmmm}^{(3)}}{I_m^{(2)}} + \frac{I_{mmnn}^{(4)} + 4I_{mnmn}^{(4)} + I_{nnmm}^{(4)} - \left(\omega_m^2 + \omega_n^2\right)I_{mnmn}^{(3)}}{I_m^{(2)}} \frac{A_n^2}{A_m^2} \right), \tag{A21}$$

with the second equation again obtained by swapping m and n; these solutions are independent of the phases, ϕ_m and ϕ_n.

The resonant frequencies are then expressed in terms of the small parameter, $\epsilon \equiv (A/L)^2 \ll 1$, where $A \equiv \max(A_m, A_n)$, i.e.,

$$\omega_i = \omega_i^{(0)} \left(1 + \frac{\Delta \omega_i}{\omega_i^{(0)}}\right), \quad i = m, n, \tag{A22}$$

with $\Delta \omega_i / \omega_i^{(0)} = \epsilon\, \delta \omega_i (1 + O(\epsilon))$ and $\delta \omega_i = O(1)$, which is substituted into Eq. (A21) and expanded in small ϵ, to give the required leading-order result in the small-amplitude limit,

$$\frac{\Delta \omega_m}{\omega_m^{(0)}} = X_m \left(\frac{A_m}{L}\right)^2 + (1 - \delta_{mn}) V_{mn} \left(\frac{A_n}{L}\right)^2, \tag{A23}$$

where δ_{mn} is the Kronecker delta function, and

$$X_m = \frac{3I_{mmmm}^{(4)}}{I_m^{(2)}} - \frac{I_{mmmm}^{(3)}}{4I_m^{(1)}}, \quad V_{mn} = \frac{I_{mmnn}^{(4)} + 4I_{mnmn}^{(4)} + I_{nnmm}^{(4)}}{4I_m^{(2)}} - \left(1 + \frac{I_n^{(2)}}{I_n^{(1)}} \frac{I_m^{(1)}}{I_m^{(2)}}\right) \frac{I_{mnmn}^{(3)}}{4I_m^{(1)}}. \tag{A24}$$

[1] J. Chaste, A. Eichler, J. Moser, G. Ceballos, R. Rurali, and A. Bachtold, A nanomechanical mass sensor with yoctogram resolution, Nat. Nanotechnol. **7**, 301 (2012).

[2] M. M. Stevens, C. L. Maire, N. Chou, M. A. Murakami, D. S. Knoff, Y. Kikuchi, R. J. Kimmerling, H. Liu, S. Haidar, N. L. Calistri, N. Cermak, S. Olcum, N. A. Cordero, A. Idbaih, P. Y. Wen, D. M. Weinstock, K. L. Ligon, and S. R. Manalis, Drug sensitivity of single cancer cells is predicted by changes in mass accumulation rate, Nat. Biotechnol. **34**, 1161 (2016).

[3] M. Gagino, G. Katsikis, S. Olcum, L. Virot, M. Cochet, A. Thuaire, S. R. Manalis, and V. Agache, Suspended nanochannel resonator arrays with piezoresistive sensors for high-throughput weighing of nanoparticles in solution, ACS Sens. **5**, 1230 (2020).

[4] R. Calmo, A. Lovera, S. Stassi, A. Chiadò, D. Scaiola, F. Bosco, and C. Ricciardi, Monolithic glass suspended microchannel resonators for enhanced mass sensing of liquids, Sens. Actuators B **283**, 298 (2019).

[5] S. Stassi, I. Cooperstein, M. Tortello, C. F. Pirri, S. Magdassi, and C. Ricciardi, Reaching silicon-based NEMS performances with 3D printed nanomechanical resonators, Nat. Commun. **12**, 6080 (2021).

[6] F.-R. Lamberti, U. Palanchoke, T. P. J. Geurts, M. Gely, S. Regord, L. Banniard, M. Sansa, I. Favero, G. Jourdan, and S. Hentz, Real-time sensing with multiplexed optomechanical resonators, Nano Lett. **22**, 1866 (2022).

[7] I. Stachiv, Z. Machů, O. Ševeček, O. Tuhovcak, M. Kotoul, and Y.-R. Jeng, Resolving measurement of large ($\sim$ GDa) chemical/biomolecule complexes with multimode nanomechanical resonators, Sens. Actuators B **353**, 131062 (2022).

[8] K. L. Ekinci, Y. T. Yang, and M. L. Roukes, Ultimate limits to inertial mass sensing based upon nanoelectromechanical systems, J. Appl. Phys. **95**, 2682 (2004).

[9] E. Sage, M. Sansa, S. Fostner, M. Defoort, M. Gély, A. K. Naik, R. Morel, L. Duraffourg, M. L. Roukes, T. Alava, G. Jourdan, E. Colinet, C. Masselon, A. Brenac, and S. Hentz, Single-particle mass spectrometry with arrays of frequency-addressed nanomechanical resonators, Nat. Commun. **9**, 3283 (2018).

[10] A. K. Naik, M. S. Hanay, W. K. Hiebert, X. L. Feng, and M. L. Roukes, Towards single-molecule nanomechanical mass spectrometry, Nat. Nanotechnol. **4**, 445 (2009).

[11] E. Sage, A. Brenac, T. Alava, R. Morel, C. Dupré, M. S. Hanay, M. L. Roukes, L. Duraffourg, C. Masselon, and S. Hentz, Neutral particle mass spectrometry with nanomechanical systems, Nat. Commun. **6**, 6482 (2015).

[12] M. S. Hanay, S. Kelber, A. K. Naik, D. Chi, S. Hentz, E. C. Bullard, E. Colinet, L. Duraffourg, and M. L. Roukes, Single-protein nanomechanical mass spectrometry in real time, Nat. Nanotechnol. **7**, 602 (2012).

[13] M. Sansa, M. Defoort, A. Brenac, M. Hermouet, L. Banniard, A. Fafin, M. Gely, C. Masselon, I. Favero, G. Jourdan, and S. Hentz, Optomechanical mass spectrometry, Nat. Commun. **11**, 3781 (2020).

[14] O. Malvar, J. J. Ruz, P. M. Kosaka, C. M. Domínguez, E. Gil-Santos, M. Calleja, and J. Tamayo, Mass and stiffness spectrometry of nanoparticles and whole intact bacteria by multimode nanomechanical resonators, Nat. Commun. **7**, 13452 (2016).

[15] J. E. Sader, M. S. Hanay, A. P. Neumann, and M. L. Roukes, Mass spectrometry using nanomechanical systems: Beyond the point-mass approximation, Nano Lett. **18**, 1608 (2018).

[16] M. S. Hanay, S. I. Kelber, C. D. O'Connell, P. Mulvaney, J. E. Sader, and M. L. Roukes, Inertial imaging with nanomechanical systems, Nat. Nanotechnol. **10**, 339 (2015).

[17] S. Stassi, G. De Laurentis, D. Chakraborty, K. Bejtka, A. Chiodoni, J. E. Sader, and C. Ricciardi, Large-scale parallelization of nanomechanical mass spectrometry with weakly-coupled resonators, Nat. Commun. **10**, 3647 (2019).

[18] E. Gil-Santos, J. J. Ruz, O. Malvar, I. Favero, A. Lemaître, P. M. Kosaka, S. García-López, M. Calleja, and J. Tamayo, Optomechanical detection of vibration modes of a single bacterium, Nat. Nanotechnol. **15**, 469 (2020).

[19] K. Asadi, J. Yu, and H. Cho, Nonlinear couplings and energy transfers in micro- and nano-mechanical resonators: Intermodal coupling, internal resonance and synchronization, Philos. Trans. R. Soc. A **376**, 20170141 (2018).

[20] R. Lifshitz and M. C. Cross, Nonlinear dynamics of nanomechanical and micromechanical resonators, in *Reviews of Nonlinear Dynamics and Complexity* (John Wiley & Sons, Ltd., New York, 2008), Chap. 1, pp. 1–52.

[21] S. Olcum, N. Cermak, S. C. Wasserman, and S. R. Manalis, High-speed multiple-mode mass-sensing resolves dynamic nanoscale mass distributions, Nat. Commun. **6**, 7070 (2015).

[22] J. F. Collis, S. Olcum, D. Chakraborty, S. R. Manalis, and J. E. Sader, Measurement of navier slip on individual nanoparticles in liquid, Nano Lett. **21**, 4959 (2021).

[23] E. Kenig, M. C. Cross, L. G. Villanueva, R. B. Karabalin, M. H. Matheny, R. Lifshitz, and M. L. Roukes, Optimal operating points of oscillators using nonlinear resonators, Phys. Rev. E **86**, 056207 (2012).

[24] L. G. Villanueva, R. B. Karabalin, M. H. Matheny, E. Kenig, M. C. Cross, and M. L. Roukes, A nanoscale parametric feedback oscillator, Nano Lett. **11**, 5054 (2011).

[25] L. G. Villanueva, E. Kenig, R. B. Karabalin, M. H. Matheny, R. Lifshitz, M. C. Cross, and M. L. Roukes, Surpassing fundamental limits of oscillators using nonlinear resonators, Phys. Rev. Lett. **110**, 177208 (2013).

[26] N. Kacem, J. Arcamone, F. Perez-Murano, and S. Hentz, Dynamic range enhancement of nonlinear nanomechanical resonant cantilevers for highly sensitive NEMS gas/mass sensor applications, J. Micromech. Microeng. **20**, 045023 (2010).

[27] L. G. Villanueva, R. B. Karabalin, M. H. Matheny, D. Chi, J. E. Sader, and M. L. Roukes, Nonlinearity in nanomechanical cantilevers, Phys. Rev. B **87**, 024304 (2013).

[28] W. J. Venstra, M. J. Capener, and S. R. Elliott, Nanomechanical gas sensing with nonlinear resonant cantilevers, Nanotechnology **25**, 425501 (2014).

[29] H. J. R. Westra, M. Poot, H. S. J. van der Zant, and W. J. Venstra, Nonlinear modal interactions in clamped-clamped mechanical resonators, Phys. Rev. Lett. **105**, 117205 (2010).

[30] A. Eichler, M. del Álamo Ruiz, J. A. Plaza, and A. Bachtold, Strong coupling between mechanical modes in a nanotube resonator, Phys. Rev. Lett. **109**, 025503 (2012).

[31] M. Matheny, L. Villanueva, R. Karabalin, J. E. Sader, and M. L. Roukes, Nonlinear mode-coupling in nanomechanical systems, Nano Lett. **13**, 1622 (2013).

[32] I. Mahboob, N. Perrissin, K. Nishiguchi, D. Hatanaka, Y. Okazaki, A. Fujiwara, and H. Yamaguchi, Dispersive and dissipative coupling in a micromechanical resonator embedded with a nanomechanical resonator, Nano Lett. **15**, 2312 (2015).

[33] A. B. Arı, M. Çağatay Karakan, C. Yanık, İ. İ. Kaya, and M. Selim Hanay, Intermodal coupling as a probe for detecting nanomechanical modes, Phys. Rev. Appl. **9**, 034024 (2018).

[34] S. Cho, S. U. Cho, M. Jo, J. Suh, H. C. Park, S. G. Kim, S.-B. Shim, and Y. D. Park, Strong two-mode parametric interaction and amplification in a nanomechanical resonator, Phys. Rev. Appl. **9**, 064023 (2018).

[35] H. J. R. Westra, H. S. J. van der Zant, and W. J. Venstra, Modal interactions of flexural and torsional vibrations in a microcantilever, Ultramicroscopy **120**, 41 (2012).

[36] T. Zhang, J. Ren, X. Wei, Z. Jiang, and R. Huan, Nonlinear coupling of flexural mode and extensional bulk mode in micromechanical resonators, Appl. Phys. Lett. **109**, 224102 (2016).

[37] A. Chandrashekar, P. Belardinelli, S. Lenci, U. Staufer, and F. Alijani, Mode coupling in dynamic atomic force microscopy, Phys. Rev. Appl. **15**, 024013 (2021).

[38] M. Hamdan and N. Shabaneh, On the large amplitude free vibrations of a restrained uniform beam carrying an intermediate lumped mass, J. Sound Vib. **199**, 711 (1997).